ACS Catalysis

Letter

pubs.acs.org/acscatalysis

Synthesis and Catalytic Activity of Sn-MFI Nanosheets for the Baeyer–Villiger Oxidation of Cyclic Ketones

Helen Y. Luo, Linh Bui, William R. Gunther, Elizabeth Min, and Yuriy Román-Leshkov*

Department of Chemical Engineering, Massachusetts Institute of Technology, Cambridge, Massachusetts 02139, United States

Supporting Information

ABSTRACT: Stannosilicate zeolites with nanosheet morphology and MFI topology (Sn-MFI-ns) are successfully synthesized with an amphiphilic organic structure-directing agent. Sn source, Si/Sn ratio, crystallization time and temperature impact framework Sn incorporation and nanosheet morphology. Optimal synthesis conditions generate Sn-MFI-ns with high crystallinity and isolated framework Sn sites. Nanosheets are ~2 nm thick in the (010) direction, resulting in large intersheet mesopore volumes and external surface areas exceeding 430 m^2/g. Unlike bulk Sn-MFI, Sn-MFI-ns is highly active in the Baeyer–Villiger oxidation of bulky cyclic ketones using hydrogen peroxide (H_2O_2). Although Sn-MFI-ns and Sn-MCM-41 have comparable activity and oxidant efficiency, the nanosheets exhibit drastically higher thermal and hydrothermal stability.

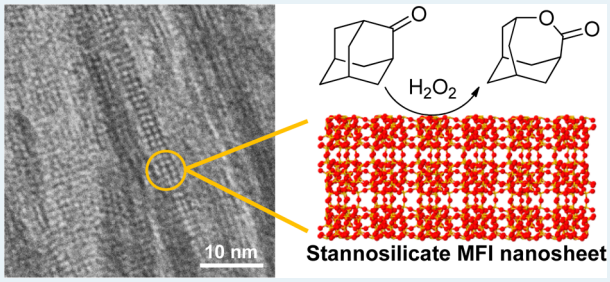

KEYWORDS: *zeolite nanosheets, Baeyer–Villiger oxidation, Sn-MFI, solid Lewis acid*

Zeolites are highly active and selective heterogeneous catalysts used in many important chemical processes.[1] The microporous crystalline frameworks of most aluminosilicates have high hydrothermal stability and feature attractive shape and transition-state selectivity effects. However, in some cases, microporosity hinders the diffusion of bulky molecules, resulting in lowered catalyst activity and faster deactivation. Hierarchical zeolites that contain open mesoporous/microporous architectures have emerged as novel materials that improve traffic of reactants and products by drastically shortening intracrystalline diffusional paths. Hierarchical zeolites have been obtained by desilication[2,3] or dealumination,[4] by exfoliation[5,6] or pillaring[7,8] of layered zeolites, and by growth of zeolites in hard templates.[9]

Recently, a novel synthetic approach was reported by Ryoo and co-workers wherein zeolite nanosheets with single-unit-cell thickness are obtained in aggregates that retain a high intersheet mesopore volume after calcination.[10] This is accomplished using surfactant-like organic structure-directing agents (SDAs) consisting of a paraffinic hydrophobic tail and a hydrophilic head containing diquaternary amines spaced at regular intervals. The head directs the formation of the zeolite while the tail prevents crystal growth in one spatial dimension. Aluminosilicate nanosheets have shown high catalytic activity in Friedel–Crafts alkylation of bulky substrates and increased catalytic lifetime during the methanol-to-olefins reaction.[6,10,11] In addition, the titanosilicate version has shown high reactivity and selectivity for the epoxidation of bulky olefins.[12]

Lewis acids play a central role in the selective activation of functional groups in organic and biochemical transformations. Tetravalent tin (Sn^{4+}) centers incorporated into zeolite frameworks are highly active solid Lewis acid catalysts.[13] For example, Sn-Beta (i.e., a zeolite with the Beta topology containing isolated Sn^{4+} sites) has been used in several important reactions, including Baeyer–Villiger (BV) oxidations,[14] Meerwein–Ponndorf–Verley reductions,[15] and isomerizations of biomass-derived carbohydrates.[16−19] In addition, mesoporous tin-containing silicates, such as Sn-MCM-41, have been used for acetalization of glycerol,[20] conversion of trioses to lactates,[21,22] Mukaiyama-aldol condensations[23] and catalytic cellulose pyrolysis.[24] Demanding applications, such as the conversion of lignocellulosic biomass and the production of fine chemicals, require hydrothermally stable catalysts capable of activating bulky substrates. Emerging zeolite nanosheet materials are ideal for providing highly active catalysts with the required open architectures to allow the interaction of large molecules with active sites.

Here we report on the synthesis, catalytic activity, and hydrothermal stability of stannosilicate zeolite nanosheets with MFI topology (Sn-MFI-ns) using the BV oxidation of bulky cyclic ketones as a test reaction. The impact of various synthesis variables on nanosheet crystallization and framework Sn incorporation was investigated with the aim of maximizing crystallinity and tetrahedral Sn content while preserving nanosheet morphology. Specifically, we studied Si/Sn ratios of 125, 167, and 250; crystallization temperatures of 423 and 433 K; and crystallization time periods ranging between 10 and 20 days using two types of Sn precursors.

Received: August 9, 2012
Revised: October 23, 2012
Published: October 31, 2012

 © 2012 American Chemical Society dx.doi.org/10.1021/cs300543z | *ACS Catal.* 2012, 2, 2695–2699

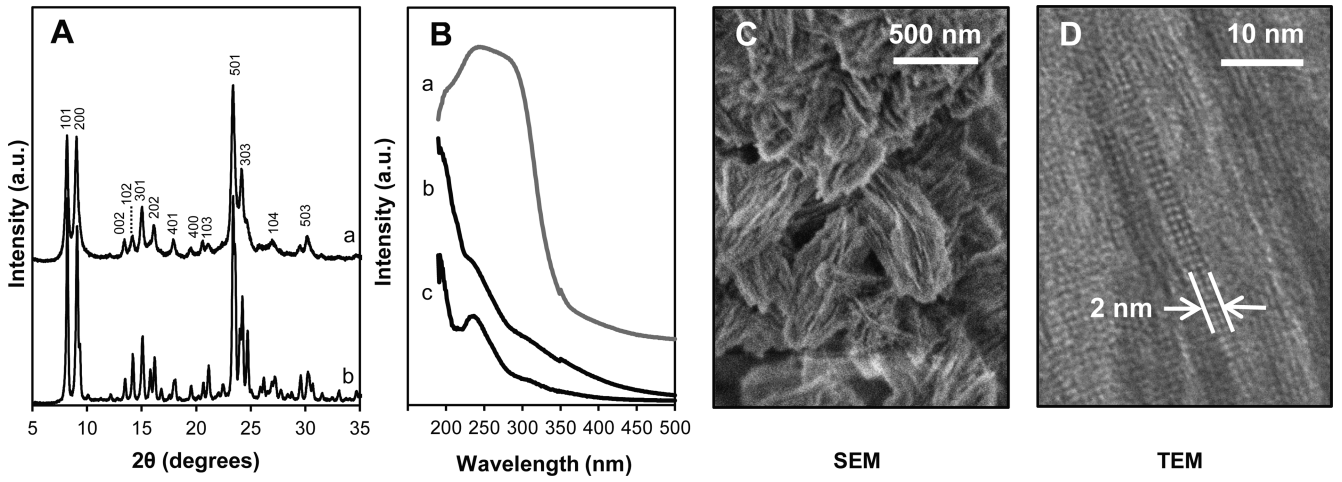

Figure 1. Characterization data of tin-containing materials calcined at 873 K. (A) PXRD patterns of (a) Sn-MFI-ns and (b) bulk Sn-MFI; (B) DR-UV spectra of (a) SnO_2 reference, (b) Sn-MFI-ns, (c) Sn-MFI-ns containing extra-framework tin synthesized with tin(IV) *tert*-butoxide; (C) SEM image of Sn-MFI-ns; (D) TEM image of Sn-MFI-ns.

Sn-MFI-ns catalysts were hydrothermally synthesized using tetraethylorthosilicate (TEOS) as the silica precursor, tin(IV) chloride pentahydrate (Sn−Cl) or tin(IV) *tert*-butoxide (Sn-but) as the tin precursor, and a dual porogenic surfactant with formula $C_{16}H_{33}-N^+(CH_3)_2-C_6H_{12}-N^+(CH_3)_2-C_6H_{13}$ as the SDA. Typical molar gel compositions were 1 SiO_2/(0.1−0.13) SDA/(0.004−0.008) SnO_2/60 H_2O. Detailed synthesis procedures can be found in the Supporting Information. The amount and type of Sn precursor used and the crystallization temperature had the strongest impact on nanosheet formation. Optimal Sn-MFI-ns syntheses were accomplished using Sn−Cl, with Si/Sn ratios >167 and a temperature of 423 K. Characterization data for these solids are shown in Figure 1. Powder X-ray diffraction (PXRD) data confirm the presence of the MFI topology, but the diffraction pattern for Sn-MFI-ns features broader peaks than those observed for bulk MFI crystals and contains reflections primarily belonging to (*h*0*l*) directions (see Figure 1A). Simulated diffraction patterns, obtained using UDSKIP, for MFI crystal fragments that are 10 unit cells wide along the *a*- and *c*-axes and one unit cell thick along the *b*-axis are in good agreement with the experimental Sn-MFI-ns PXRD patterns (Supporting Information Figure S20). As expected, the simulation shows considerable peak-broadening and a dramatic decrease in peak intensity for reflections associated with long-range order along the *b*-axis.

Similar results have been reported for hierarchical zeolites featuring structural properties analogous to those of Sn-MFI-ns.[8,10] Diffuse-reflectance ultraviolet (DR-UV) spectrometry shows a single adsorption band centered at ∼200 nm, indicating that most Sn atoms are tetrahedrally incorporated into the zeolite framework (Figure 1B). In contrast, when Sn-but is used as the Sn source, a band centered at ∼245 nm is consistently observed, regardless of the Si/Sn ratio or crystallization temperature used.

Scanning electron microscopy (SEM) and transmission electron microscopy (TEM) were used to probe the structure and morphology of the nanosheets. SEM images of Sn-MFI-ns revealed uniform particles composed of disordered platelets agglomerated into 500 nm ovoidal structures (Figure 1C). No other apparent morphologies were detected during low-magnification inspections. TEM imaging confirmed the presence of lamellae ∼2 nm thick along the (010) direction and ∼100 nm long along the (100) and (001) directions (Figures 1D and Supporting Information Figure SC). To further confirm the absence of mixed phases, a physical mixture of crystalline bulk Sn-MFI and amorphous Sn-MCM-41 (1:4 w/w ratio) was characterized and compared to Sn-MFI-ns (Supporting Information Figures S18 and S19). SEM images and PXRD patterns of the physical mixture are drastically different from those obtained for Sn-MFI-ns. Specifically, SEM images of the mixture clearly show the presence of ∼250 nm crystals covered in amorphous material, and the PXRD pattern is interpreted as a distinct superimposition of the patterns of MFI crystals and amorphous silica.

Argon adsorption isotherms at 87.3 K and pore size analysis are presented in Figure 2. The cumulative pore volume calculated using nonlocal density functional theory (NLDFT) up to a 50 nm pore indicates the presence of both meso- and microporosity in the Sn-MFI-ns sample (Figure 2B). The pore size distribution, also plotted up to 50 nm, indicates micropores centered at 0.522 nm and a very broad distribution of mesopores from 5 to 20 nm. The total micropore volume

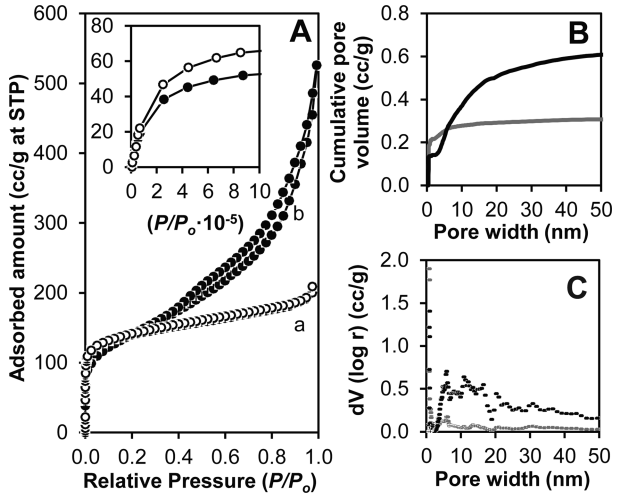

Figure 2. (A) Argon adsorption isotherms at 87.3 K of (a) bulk Sn-MFI, (b) Sn-MFI-ns; (B) NLDFT cumulative pore volume; (C) pore size distributions of bulk Sn-MFI (gray) and Sn-MFI-ns (black).

dx.doi.org/10.1021/cs300543z | *ACS Catal.* 2012, 2, 2695−2699

and external surface area of Sn-MFI-ns after calcination are 0.135 $cm^3\ g^{-1}$ and 437 $m^2\ g^{-1}$, respectively. The micropore volume is slightly smaller than that of bulk Sn-MFI, which is 0.155 $cm^3\ g^{-1}$ (Supporting Information Table S1), and the external surface area is in good agreement with a theoretical surface area calculated using geometric arguments (Supporting Information Table SC).

Increasing the tin content in the synthesis gel leads to slower crystallization times as well as decreased crystallinity and changed morphology (Supporting Information Table S2 and Figures S1–S2). A gel containing a Si/Sn ratio of 125 not only required 44 days to crystallize at 423 K, but also resulted in a solid with more amorphous content with a visible (133) reflection in the PXRD pattern. We hypothesize that an increased amount of Cl^- ions negatively interacts with the SDA and disrupts unilamellar organization of the surfactant tails. When the tin source was changed to Sn-but, all materials contained large amounts of extraframework tin, even for the lowest Si/Sn ratio of 250 (Figures 1B and Supporting Information S6), suggesting a systematic prevalence of extraframework octahedral Sn species when this precursor is used under the synthesis conditions investigated. Increasing the synthesis temperature to 433 K decreased crystallization times considerably but mostly led to the formation of small crystalline domains embedded in a spongelike amorphous matrix regardless of the Si/Sn ratio or tin source used (Supporting Information Figures S3–5, S18). The Sn-MFI-ns chosen for catalytic investigation was synthesized with a Si/Sn of 167, the Sn–Cl tin source, and crystallization temperature of 423 K for 20 days (Supporting Information Table S2, entry 2).

The catalytic activity of various stannosilicates, including Sn-MFI-ns, Sn-MFI, Sn-Beta, and Sn-MCM-41, was evaluated using the BV oxidation of cyclic ketones as a test reaction (Figure 3 and Table 1). Sn-MFI-ns was active in the oxidation

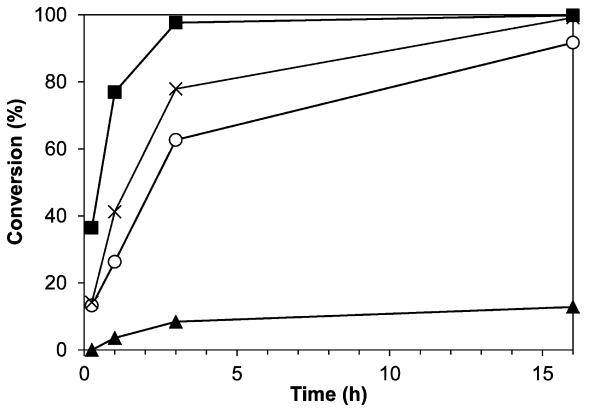

Figure 3. Conversion of 2-adamantanone with Sn-containing catalysts. Reaction conditions: catalyst, 0.66 mol % of Sn with respect to the ketone; ketone, 1 mmol; 50 wt % H_2O_2, 1.5 mmol; dioxane, 3 g; 348 K, 16 h. Catalyst legend: ■, Sn-Beta; ×, Sn-MCM-41; ○, Sn-MFI-ns; ▲, bulk Sn-MFI.

of 2-adamantanone into the corresponding lactone, achieving 92% conversion in 24 h with >98% selectivity when using 1.5 equivalents of H_2O_2 (50% aqueous solution). These values correspond to a turnover number (TON) of 122. In contrast, bulk Sn-MFI is mostly inactive, converting only 13% of the starting reagent under equal reaction conditions. These data suggest that 2-adamantanone is too large to enter the 10-membered ring pores of bulk Sn-MFI (0.54 × 0.56 nm) but is capable of reacting on the surface sites of Sn-MFI-ns.

Table 1. Catalytic Activity of Sn-Containing Catalysts for the Baeyer–Villiger Oxidation of 2-Adamantanone using H_2O_2[a]

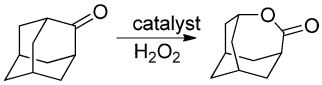

catalyst	H_2O_2[b] (equiv)	C[c] (%)	E[d] (%)	TON[e]	TOF[f] (h^{-1})	S[g] (%)
bulk Sn-MFI	1.5	13	13	17	5	95
bulk Sn-Beta	1.5	99	92	143	210	>98
Sn-MCM-41	1.5	99	82	137	58	>98
Sn-MFI-ns	1.5	92	88	122	38	>98
Sn-MFI-ns-e[h]	1.5	87	75	120	37	>98
bulk Sn-MFI	0.6	15	28	23	9	>98
Sn-MCM-41	0.6	62	99	99	91	>98
Sn-MFI-ns	0.6	62	99	104	86	>98
Sn-MFI-ns-sil[i]	1.5	39	49	51	12	>98
Sn-MCM-41-sil	1.5	76	68	91	20	>98
SnO_2-MCM-41	1.5	3	3	4	2	96

[a]Reaction conditions: catalyst, 0.66 mol % of Sn with respect to the ketone; ketone, 1 mmol; 50% H_2O_2, 1.5 or 0.6 mmol; dioxane, 3 g; 348 K, 16 h. [b]H_2O_2 equivalents with respect to ketone. [c]Conversion = (moles of ketone converted)/(initial moles of ketone) × 100. [d]Oxidant efficiency = (moles of ketone converted)/(moles of H_2O_2 consumed) × 100. [e]TON = (moles of substrate converted)/(moles of tin centers) at 16 h. [f]TOF = (moles of substrate converted)/(moles of tin centers) per hour calculated from 1 h conversions, except Sn-Beta at 15 min. [g]Selectivity = (moles of product)/(moles of ketone reacted) × 100. [h]"-e" indicates the presence of extraframework tin. [i]"-sil" indicates the catalyst is silylated.

Hydrophobic zeolites with isolated Lewis acid sites are preferred catalysts for BV oxidations because water is known to negatively impact Lewis acidity.[13] However, Sn-MCM-41 and Sn-MFI-ns are hydrophilic materials because their surfaces are terminated in hydroxyl groups. Our catalytic tests show that a hydrophobic, defect-free Sn-Beta zeolite synthesized in fluoride media has higher reactivity (TOF = 210 h^{-1}) and H_2O_2 efficiency (E = 92%) than Sn-MCM-41 (TOF = 58 h^{-1}, E = 82%) or Sn-MFI-ns (TOF = 38 h^{-1}, E = 88%). Note that all TOFs are calculated using total Sn atoms rather than external Sn atoms. We hypothesize that the reduced catalytic activity of the external surface tin sites in Sn-MFI-ns when compared with the internal tin sites of Sn-Beta is due to the lack of pore-confining effects or a more pronounced competitive binding of water to the hydrophilic surface of Sn-MFI-ns. This is further evidenced by the similar catalytic behavior observed for Sn-MCM-41 and Sn-MFI-ns with a cyclic ketone that is more difficult to oxidize. Specifically, the oxidation activity of Sn-MFI-ns and Sn-MCM-41 is much lower for cyclohexanone when compared with Sn-Beta (Supporting Information Table S3 and Figure S8). This result is expected and is attributed to the decreased capacity of surface Sn sites to activate cyclic ketones with secondary carbons when compared with active sites located inside the pores of Beta. Note that when the water content is decreased by using H_2O_2-deficient reactions conditions (i.e., 0.6 equiv), the efficiency of both Sn-MFI-ns and Sn-MCM-41 is nearly 100% and TOFs increase to 86 and 91 h^{-1}, respectively. These results prompted us to decrease hydrophilicity by silylating the surfaces with triethoxymethylsilane. Unfortunately, catalytic activity after silylation was

dx.doi.org/10.1021/cs300543z | ACS Catal. 2012, 2, 2695–2699

reduced for both materials, likely because of blocking of surface active sites (Table 1).

The presence of extraframework tin sites leads to reduced activity because SnO_2 is inactive for the BV oxidation. Thus, SnO_2 supported on Si-MCM-41 yielded negligible 2-adamantanone conversion. Consequently, Sn-MFI-ns synthesized using Sn-but (i.e., containing extraframework tin) showed decreased activity and lower H_2O_2 efficiency when compared with Sn-MFI-ns synthesized with Sn−Cl. Clearly, framework tin incorporation and framework tin stability are critical factors to obtain an efficient catalyst. Our results show that tin atoms, once incorporated in the framework, do not leach into solution or convert to extraframework species. Specifically, recyclability tests showed a progressive decrease in catalytic activity after each 16 h cycle; however, the catalyst regained most of its initial activity after recalcining at 823 K (see Supporting Information Figure S17). Corma and co-workers reported a similar behavior for Sn-MCM-41 and attributed deactivation to product remaining absorbed on the catalyst after the reaction.[25] To check for the possibility of leaching, an experiment was carried out in which Sn-MFI-ns was separated by hot filtration after 1 h (21% conversion). After heating the filtrate for an additional 5 h, the conversion did not increase further. Elemental analysis using inductively coupled plasma (ICP) atomic emission spectroscopy of the sample before and after reaction did not show a change in tin content.

Importantly, stability tests reveal that Sn-MFI-ns exhibits higher thermal and hydrothermal stability when compared with Sn-MCM-41 (Figure 4 and Supporting Information Table S4).

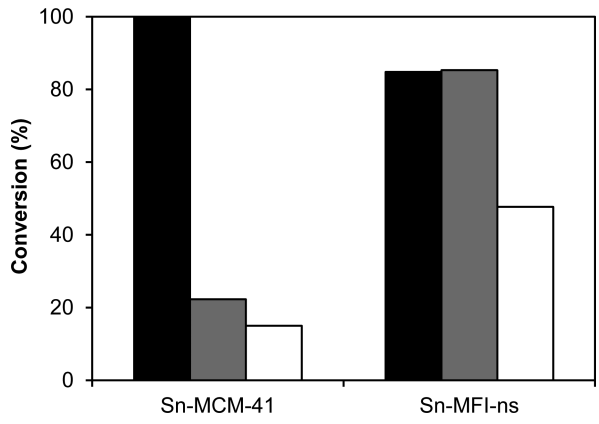

Figure 4. Conversion of 2-adamantanone at 16 h after thermal/hydrothermal treatments for materials: calcined at 823 K (black), calcined at 1273 K (gray), treated in water at 403 K for 6 h (white). Note: the Sn-MFI-ns subjected to the hydrothermal treatment was first subjected to the thermal treatment at 1273 K. Reaction conditions: catalyst, 0.66 mol % of Sn with respect to the ketone; ketone, 1 mmol; 50 wt % H_2O_2, 1.5 mmol; dioxane, 3 g; 348 K, 16 h.

Specifically, thermally treating a Sn-MCM-41 sample at 1273 K for 4 h resulted in a decrease in surface area from 900 to 53 m^2/g with a concomitant decrease in oxidation activity of 78%. PXRD confirmed collapse of the mesoporous structure after the thermal treatment. Similarly, a pristine Sn-MCM-41 sample subjected to a hydrothermal treatment consisting of stirring the catalyst in water at 403 K for 6 h in a sealed vial resulted in a decrease in the surface area from 900 to 282 m^2/g and a loss in reactivity of 84%. In contrast, a Sn-MFI-ns sample subjected to the same thermal treatment preserved 95% of its original surface area and 100% of its oxidation activity. After subjecting the thermally treated sample to the hydrothermal treatment, a decrease in surface area from 469 to 367 m^2/g was observed, resulting in a decrease in activity of 43% with respect to the pristine material. The superior thermal and hydrothermal stability of Sn-MFI-ns with respect to Sn-MCM-41 is likely due to the crystalline nature of the framework.

In summary, Sn-MFI-ns was successfully synthesized under optimal conditions of tin source, tin content, and crystallization temperature. The best materials, featuring fully crystalline structures and mainly tetrahedrally coordinated tin had Si/Sn ratios >167, used Sn−Cl as the tin source, and were crystallized at 423 K. Sn-MFI-ns showed a significant increase in catalytic activity for the BV oxidation of cyclic ketones compared with bulk Sn-MFI. The activities and efficiencies strongly matched those of Sn-MCM-41, indicating the external Sn sites in Sn-MFI-ns have a performance similar to Sn sites embedded in a mesoporous amorphous silica framework. Sn-MFI-ns showed superior thermal and hydrothermal stability when compared with Sn-MCM-41. Indeed, zeolite nanosheets are a novel class of catalysts with open crystalline architectures that provide large organic molecules with free access to the active sites. In addition, these materials also offer a high surface area scaffold that can be used to tether organic molecules. Future investigations should be geared at understanding the differences in reactivity between external and internal sites and at exploiting the large surface areas to create novel multifunctional hybrid organic−inorganic catalysts.

■ ASSOCIATED CONTENT

Supporting Information

Zeolite synthesis conditions; detailed experimental procedures for catalytic testing; characterization (adsorption isotherms, PXRD, ICP, TEM, SEM images), and additional results of catalytic reactions. This material is available free of charge via the Internet at http://pubs.acs.org.

■ AUTHOR INFORMATION

Corresponding Author

*E-mail: yroman@mit.edu.

Notes

The authors declare no competing financial interest.

■ ACKNOWLEDGMENTS

W.R.G. gratefully acknowledges support from the National Science Foundation MIT Center for Materials Science and Engineering (DMR-0819762). L.B. and E.M. thank MIT's Undergraduate Research Opportunities Program (UROP) and the MIT Energy Initiative for funding. We thank the MIT Center for Materials Science and Engineering for assistance in taking TEM images in their microscopy facilities.

■ REFERENCES

(1) Corma, A. *Chem. Rev.* **1997**, *97*, 2373−2420.
(2) Groen, J. C.; Zhu, W.; Brouwer, S.; Huynink, S. J.; Kapteijn, F.; Moulijn, J. a; Pérez-Ramírez, J. *J. Am. Chem. Soc.* **2007**, *129*, 355−360.
(3) Groen, J. C.; Bach, T.; Ziese, U.; Paulaime-van Donk, A. M.; de Jong, K. P.; Moulijn, J. A.; Pérez-Ramírez, J. *J. Am. Chem. Soc.* **2005**, *127*, 10792−10793.
(4) Beyer, H. In *Post-Synthesis Modification I*; Springer: Berlin, Heidelberg, 2002; Vol. 3, pp 203−255.
(5) Corma, A.; Fornes, V.; Pergher, S. *Nature* **1998**, *396*, 1−4.
(6) Corma, A.; Fornes, V.; Pergher, S. *J. Catal.* **1999**, *63*, 57−63.

(7) Maheshwari, S.; Jordan, E.; Kumar, S.; Bates, F. S.; Penn, R. L.; Shantz, D. F.; Tsapatsis, M. *J. Am. Chem. Soc.* **2008**, *130*, 1507−1516.
(8) Zhang, X.; Liu, D.; Xu, D.; Asahina, S.; Cychosz, K. a; Agrawal, K. V.; Al Wahedi, Y.; Bhan, A.; Al Hashimi, S.; Terasaki, O.; Thommes, M.; Tsapatsis, M. *Science (New York, N.Y.)* **2012**, *336*, 1684−1687.
(9) Fan, W.; Snyder, M. a; Kumar, S.; Lee, P.-S.; Yoo, W. C.; McCormick, A. V.; Lee Penn, R.; Stein, A.; Tsapatsis, M. *Nature materials* **2008**, *7*, 984−991.
(10) Choi, M.; Na, K.; Kim, J.; Sakamoto, Y.; Terasaki, O.; Ryoo, R. *Nature* **2009**, *461*, 246−249.
(11) Na, K.; Jo, C.; Kim, J.; Cho, K.; Jung, J.; Seo, Y.; Messinger, R. J.; Chmelka, B. F.; Ryoo, R. *Science* **2011**, *333*, 328−332.
(12) Na, K.; Jo, C.; Kim, J.; Ahn, W.-S.; Ryoo, R. *ACS Catal.* **2011**, *1*, 901−907.
(13) Román-Leshkov, Y.; Davis, M. E. *ACS Catal.* **2011**, *1*, 1566−1580.
(14) Corma, A.; Nemeth, L. T.; Renz, M.; Valencia, S. *Nature* **2001**, *412*, 423−425.
(15) Corma, A.; Domine, M. E.; Nemeth, L.; Valencia, S. *J. Am. Chem. Soc.* **2002**, *124*, 3194−3195.
(16) Moliner, M.; Román-Leshkov, Y.; Davis, M. E. *Proc. Nat. Acad. Sci.* **2010**, *107*, 6164−6168.
(17) Román-Leshkov, Y.; Moliner, M.; Labinger, J. A.; Davis, M. E. *Angew. Chem., Int. Ed.* **2010**, *49*, 8954−8957.
(18) Holm, M. S.; Saravanamurugan, S.; Taarning, E. *Science* **2010**, *328*, 602−605.
(19) Bermejo-Deval, R.; Assary, R. S.; Nikolla, E.; Moliner, M.; Román-Leshkov, Y.; Hwang, S.-J.; Palsdottir, A.; Silverman, D.; Lobo, R. F.; Curtiss, L. a; Davis, M. E. *Proc. Natl. Acad. Sci. U. S. A.* **2012**, *109*, 9727−9732.
(20) Li, L.; Korányi, T. T. I.; Sels, B. F.; Pescarmona, P. P. *Green Chem.* **2012**, *14*, 1611.
(21) Pescarmona, P. P.; Janssen, K. P. F.; Delaet, C.; Stroobants, C.; Houthoofd, K.; Philippaerts, A.; De Jonghe, C.; Paul, J. S.; Jacobs, P. A.; Sels, B. F. *Green Chem.* **2010**, *12*, 1083−1089.
(22) de Clippel, F.; Dusselier, M.; Van Rompaey, R.; Vanelderen, P.; Dijkmans, J.; Makshina, E.; Giebeler, L.; Oswald, S.; Baron, G. V.; Denayer, J. F. M.; Pescarmona, P. P.; Jacobs, P. a; Sels, B. F. *J. Am. Chem. Soc.* **2012**, *134*, 10089−10101.
(23) Gaydhankar, T. R.; Joshi, P. N.; Kalita, P.; Kumar, R. *J. Mol. Catal. A: Chem.* **2007**, *265*, 306−315.
(24) Torri, C.; Lesci, I. G.; Fabbri, D. *J. Anal. Appl. Pyrol.* **2009**, *85*, 192−196.
(25) Corma, A.; Navarro, M. T.; Renz, M. *J. Catal.* **2003**, *219*, 242−246.